

# Complement and inflammasome overactivation mediates paroxysmal nocturnal hemoglobinuria with autoinflammation

Britta Höchsmann, ... , Peter M. Krawitz, Taroh Kinoshita

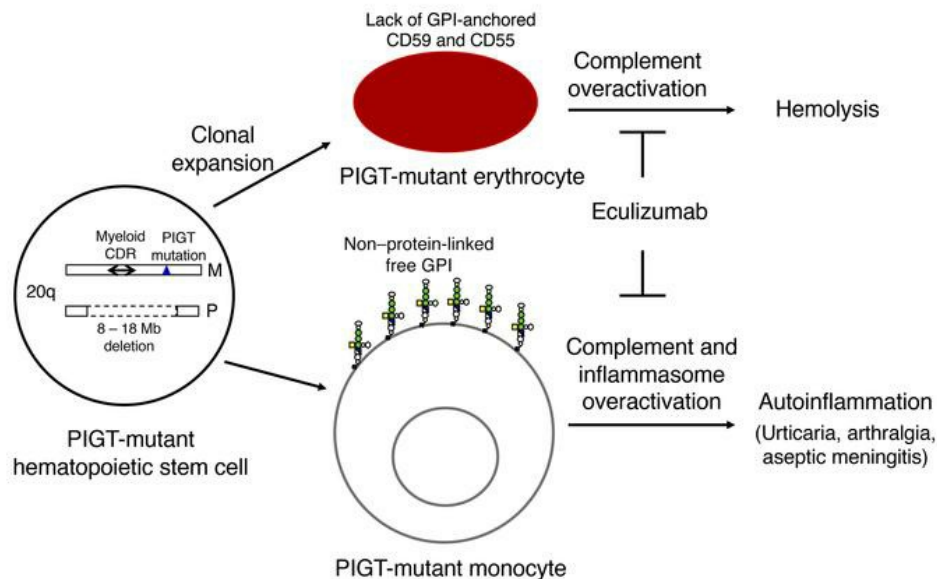
*J Clin Invest.* 2019;129(12):5123-5136. <https://doi.org/10.1172/JCI123501>.

Research Article

Hematology

Inflammation

## Graphical abstract



Find the latest version:

<https://jci.me/123501/pdf>



# Complement and inflammasome overactivation mediates paroxysmal nocturnal hemoglobinuria with autoinflammation

Britta Höchsmann,<sup>1,2</sup> Yoshiko Murakami,<sup>3,4</sup> Makiko Osato,<sup>3,5</sup> Alexej Knaus,<sup>6</sup> Michi Kawamoto,<sup>7</sup> Norimitsu Inoue,<sup>8</sup> Tetsuya Hirata,<sup>3</sup> Shogo Murata,<sup>3,9</sup> Markus Anliker,<sup>1</sup> Thomas Eggermann,<sup>10</sup> Marten Jäger,<sup>11</sup> Ricarda Floettmann,<sup>11</sup> Alexander Höllein,<sup>12</sup> Sho Murase,<sup>7</sup> Yasutaka Ueda,<sup>5</sup> Jun-ichi Nishimura,<sup>5</sup> Yuzuru Kanakura,<sup>5</sup> Nobuo Kohara,<sup>7</sup> Hubert Schrezenmeier,<sup>1</sup> Peter M. Krawitz,<sup>6</sup> and Taroh Kinoshita<sup>3,4</sup>

<sup>1</sup>Institute of Transfusion Medicine, University of Ulm, Ulm, Germany. <sup>2</sup>Institute of Clinical Transfusion Medicine and Immunogenetics, German Red Cross Blood Transfusion Service and University Hospital Ulm, Ulm, Germany. <sup>3</sup>Research Institute for Microbial Diseases and <sup>4</sup>WPI Immunology Frontier Research Center, Osaka University, Osaka, Japan. <sup>5</sup>Department of Hematology and Oncology, Graduate School of Medicine, Osaka University, Osaka, Japan. <sup>6</sup>Institute for Genomic Statistics and Bioinformatics, Rheinische Friedrich-Wilhelms-Universität Bonn, Bonn, Germany. <sup>7</sup>Department of Neurology, Kobe City Medical Center General Hospital, Kobe, Japan. <sup>8</sup>Department of Tumor Immunology, Osaka International Cancer Institute, Osaka, Japan. <sup>9</sup>Department of Hematology/Oncology, Wakayama Medical University, Wakayama, Japan. <sup>10</sup>Institute for Human Genetics, Medical Faculty, RWTH University Aachen, Aachen, Germany. <sup>11</sup>Department of Medical Genetics, Charite Hospital, University of Berlin, Berlin, Germany. <sup>12</sup>MLL Muenchener Leukaemielabor GmbH, Munich, Germany.

**Patients with paroxysmal nocturnal hemoglobinuria (PNH) have a clonal population of blood cells deficient in glycosylphosphatidylinositol-anchored (GPI-anchored) proteins, resulting from a mutation in the X-linked gene *PIGA*. Here we report on a set of patients in whom PNH results instead from biallelic mutation of *PIGT* on chromosome 20. These *PIGT*-PNH patients have clinically typical PNH, but they have in addition prominent autoinflammatory features, including recurrent attacks of aseptic meningitis. In all these patients we find a germ-line point mutation in one *PIGT* allele, whereas the other *PIGT* allele is removed by somatic deletion of a 20q region comprising maternally imprinted genes implicated in myeloproliferative syndromes. Unlike in *PIGA*-PNH cells, GPI is synthesized in *PIGT*-PNH cells and, since its attachment to proteins is blocked, free GPI is expressed on the cell surface. From studies of patients' leukocytes and of *PIGT*-KO THP-1 cells we show that, through increased IL-1 $\beta$  secretion, activation of the lectin pathway of complement and generation of C5b-9 complexes, free GPI is the agent of autoinflammation. Eculizumab treatment abrogates not only intravascular hemolysis, but also autoinflammation. Thus, *PIGT*-PNH differs from *PIGA*-PNH both in the mechanism of clonal expansion and in clinical manifestations.**

## Introduction

Paroxysmal nocturnal hemoglobinuria (PNH) is an acquired hematopoietic stem cell (HSC) disorder characterized by complement-mediated hemolysis, thrombosis, and bone marrow failure (1, 2). Affected cells harbor a somatic mutation in the *PIGA* gene, essential for the initial step in glycosylphosphatidylinositol (GPI) biosynthesis that occurs in the endoplasmic reticulum (ER) (Figure 1A, top and ref. 3). Loss of GPI biosynthesis results in the defective expression of GPI-anchored proteins (GPI-APs), including complement inhibitors CD59 and DAF/CD55 (Figure 1A, middle). The affected stem cells generate large numbers of abnormal blood cells after clonal expansion that occurs under bone mar-

row failure. The affected erythrocytes are defective in complement regulation and destroyed by the membrane attack complex (MAC or C5b-9) upon complement activation (1). Eculizumab, an anti-complement component 5 (C5) monoclonal antibody (mAb), has been used to prevent intravascular hemolysis and thrombosis (4, 5). Eculizumab binds to C5 and inhibits its activation and subsequent generation of C5b-9 complexes.

Among more than 20 genes involved in GPI biosynthesis and transfer to proteins, *PIGA* is X-linked whereas all others are autosomal (6). Because of X-linkage, one somatic mutation in *PIGA* causes GPI deficiency in both males and females (3). In contrast, 2 mutations are required for an autosomal gene, but the probability of somatic mutations in both alleles at the same locus is extremely low, which explains why GPI deficiency in most patients with PNH is caused by *PIGA* somatic mutations. Recently, we reported 2 patients with PNH whose GPI-AP deficiency was caused by germline and somatic mutations in the *PIGT* gene localized on chromosome 20q (7, 8). Both patients had a heterozygous germline loss-of-function mutation in *PIGT*, along with loss of the normal allele of *PIGT* by a deletion of 8 Mb or 18 Mb occurring in HSCs (7, 8). *PIGT*, forming a GPI transamidase complex with *PIGK*, *PIGS*, *PIGU*, and *GPAA1*, acts in the transfer of preassembled GPI to

### ► Related Commentary: p. 5074

**Authorship note:** BH, YM, and MO contributed equally to this paper. HS, PMK, and TK contributed equally to this paper.

**Conflict of interest:** HS receives research support through the University of Ulm from Novartis and Alexion Pharmaceuticals.

**Copyright:** © 2019, American Society for Clinical Investigation.

**Submitted:** July 19, 2018; **Accepted:** August 16, 2019; **Published:** October 22, 2019.

**Reference information:** *J Clin Invest.* 2019;129(12):5123–5136.

<https://doi.org/10.1172/JCI123501>.

proteins in the ER (Figure 1A, top and ref. 9). In *PIGT*-defective cells, GPI is synthesized but is not transferred to precursor proteins, resulting in GPI-AP deficiency on the cell surface (Figure 1A, bottom). We showed recently that non-protein-linked, free GPI remaining in the ER of *PIGT*-defective Chinese hamster ovary (CHO) cells is transported to and displayed on the cell surface (Figure 1A, bottom and ref. 10).

Two reported PNH patients with *PIGT* defect suffered from recurrent inflammatory symptoms that are unusual in patients with PNH (7, 8). Here, we report 2 more patients with PNH who lost *PIGT* function via a similar genetic mechanism, and present insights into the expansion of *PIGT*-defective clones common among 4 patients. We also present the integrated clinical characteristics of these 4 patients and show that *PIGT*-defective mononuclear leukocytes, but not *PIGA*-defective mononuclear leukocytes, secreted IL-1 $\beta$  in response to inflammasome activators. Using a *PIGT*-KO THP-1 cell model, we show that complement activation is enhanced on the surface of *PIGT*-defective cells leading to MAC-dependent elevated secretion of IL-1 $\beta$ . Against this background, we propose a distinct disease entity, *PIGT*-PNH.

## Results

**Case report.** Japanese patient J1 (8) and German patients G1 (7), G2, and G3 were diagnosed with PNH at the ages of 68, 49, 65, and 66, respectively. The changes in PNH clone sizes in J1, G1, and G3 after PNH diagnosis are shown in Figure 1B. They were treated with eculizumab, which effectively prevented intravascular hemolysis. Percentage of PNH cells rapidly increased after commencement of eculizumab not only in erythrocytes but also in granulocytes (Figure 1B). We reported that in G1, direct Coombs test-positive erythrocytes appeared after commencement of eculizumab treatment, suggesting extravascular hemolysis (7). Blood cell counts for G1 and G3 are shown in Supplemental Figure 1A. Before the diagnosis of PNH, J1, G1, and G3 had suffered inflammatory symptoms including urticaria, arthralgia, and fever from the ages of 30, 26, and 48, respectively (Table 1). Urticaria in J1 was associated with neutrophil infiltration (8) and that in G3 with a mixed inflammatory infiltrate (Figure 1C). J1 (8) and G3 suffered from recurrent aseptic meningitis characterized by an abundance of neutrophils in cerebrospinal fluid. Following the initiation of eculizumab treatment for hemolysis 3–5 years earlier, J1 and G3 had not suffered any episodes of meningitis (Figure 1D). Urticaria and arthralgia were also ameliorated in all 3 by eculizumab treatment. G2 had severe arteriosclerosis, which might be related to autoinflammation (Table 1); however, whether G2 had autoinflammatory symptoms is unclear and could not be confirmed because the patient passed away.

**Genetic basis of GPI-AP deficiency.** Four patients did not have *PIGA* somatic mutations but had a germline mutation in one allele of *PIGT* located on chromosome 20q: patient J1, NM\_015937 (8), c.250G>T; patient G1, c.1401-2A>G (7); patient G2, c.761\_764del-GAAA; and patient G3, c.197delA (Supplemental Figure 2A; supplemental material available online with this article; <https://doi.org/10.1172/JCI123501DS1>). These cause E84X, exon 11 skipping, frameshift after G254, and frameshift after Y66, respectively. The functional activities of variant *PIGT* found in J1 and G1 were reported to be very low (7, 11). Variants in G2 and G3 causing frameshifts should also be severely deleterious to *PIGT* function. In addition to

the germline *PIGT* mutation, all 4 had in the other allele a somatic deletion of 8–18 Mb, which includes the entire *PIGT* gene (Supplemental Figure 2B and refs. 7, 8). Therefore, in contrast to GPI-AP deficiency caused by a single *PIGA* somatic mutation in PNH, GPI-AP deficiency in all 4 is caused by a combination of germline loss-of-function *PIGT* mutation and somatic loss of the whole of normal *PIGT* in hematopoietic stem cells (Figure 2A).

**A possible mechanism of clonal expansion in *PIGT*-PNH.** Deletion of chromosome 20q represents the most common chromosomal abnormality associated with myeloproliferative disorders. The deleted region of 8–18 Mb included a myeloid common deleted region (CDR) (ref. 12 and Figure 2A). A fraction (approximately 10%) of patients with myeloproliferative neoplasm (MPN) such as polycythemia vera commonly have a deletion of 2.7 Mb in chromosome 20q (12). Moreover, a fraction (approximately 4%) of patients with myelodysplastic syndrome (MDS) also have a deletion of 2.6 Mb in this region (12). The CDR region shared by MPN and MDS spanning approximately 1.9 Mb has been called myeloid CDR (Figure 2B) and its loss was shown to be causally related to clonal expansion of the affected myeloid cells in these 20q<sup>-</sup> syndromes (13). In contrast to previous cytogenetic analysis on classical PNH cases that showed no aberrations in 20q (14, 15), one allele of the myeloid CDR was lost in PNH cells of all 4 patients (Supplemental Figure 2B and refs. 7, 8).

The tumor suppressor-like gene *L3MBTL1* and the kinase gene *SGK2* located within the myeloid CDR (Figure 2, A and B) are expressed only in the paternal allele due to gene imprinting (16). It was shown that losses of active paternal alleles of these 2 genes had a causal relationship with clonal expansion of these 20q<sup>-</sup> myeloid cells (13). *L3MBTL1* and *SGK2* transcripts were undetectable in GPI-AP-defective granulocytes from J1 and extremely low in whole blood cells from G1, whereas they were found in granulocytes from healthy individuals (Figure 2C). The transcripts of 2 unimprinted genes, *IFT52* and *MYBL2*, were detected in both GPI-AP-defective granulocytes from J1 and normal granulocytes (Figure 2C, top). The results therefore indicate that the expression of *L3MBTL1* and *SGK2* is lost in GPI-AP-defective cells in J1 and G1.

The results shown in Figure 2C also indicate that the somatically deleted region in J1 and G1 included active *L3MBTL1* and *SGK2*, so it was in the paternal chromosome. Owing to mRNA from patients G2 and G3 not being available, we determined the methylation status of the *L3MBTL1* gene using DNA from blood leukocytes, among which the large majority of cells were of the PNH phenotype. *L3MBTL1* in G1 and G3 samples was hypermethylated (Figure 2D and Supplemental Figure 3A), indicating that the myeloid CDR allele remaining in their PNH clones was imprinted. In contrast, the G2 sample was hypomethylated. It was reported that, in some MPN patients with myeloid CDR deletion, the remaining allele was hypomethylated; nevertheless, its transcription was suppressed (13). G2 might be in a similar situation, although it was not possible to draw a definitive conclusion on this by reverse transcriptase-polymerase chain reaction (RT-PCR) analysis as the patient had passed away. These results indicate that the loss of expressed myeloid CDR allele is associated with clonal expansion of *PIGT*-defective cells similar to 20q<sup>-</sup> MPN and MDS.

**Appearance of free GPI on the surface of *PIGT*-defective cells.** *PIGA* is required for the first step in GPI biosynthesis (17); therefore, no

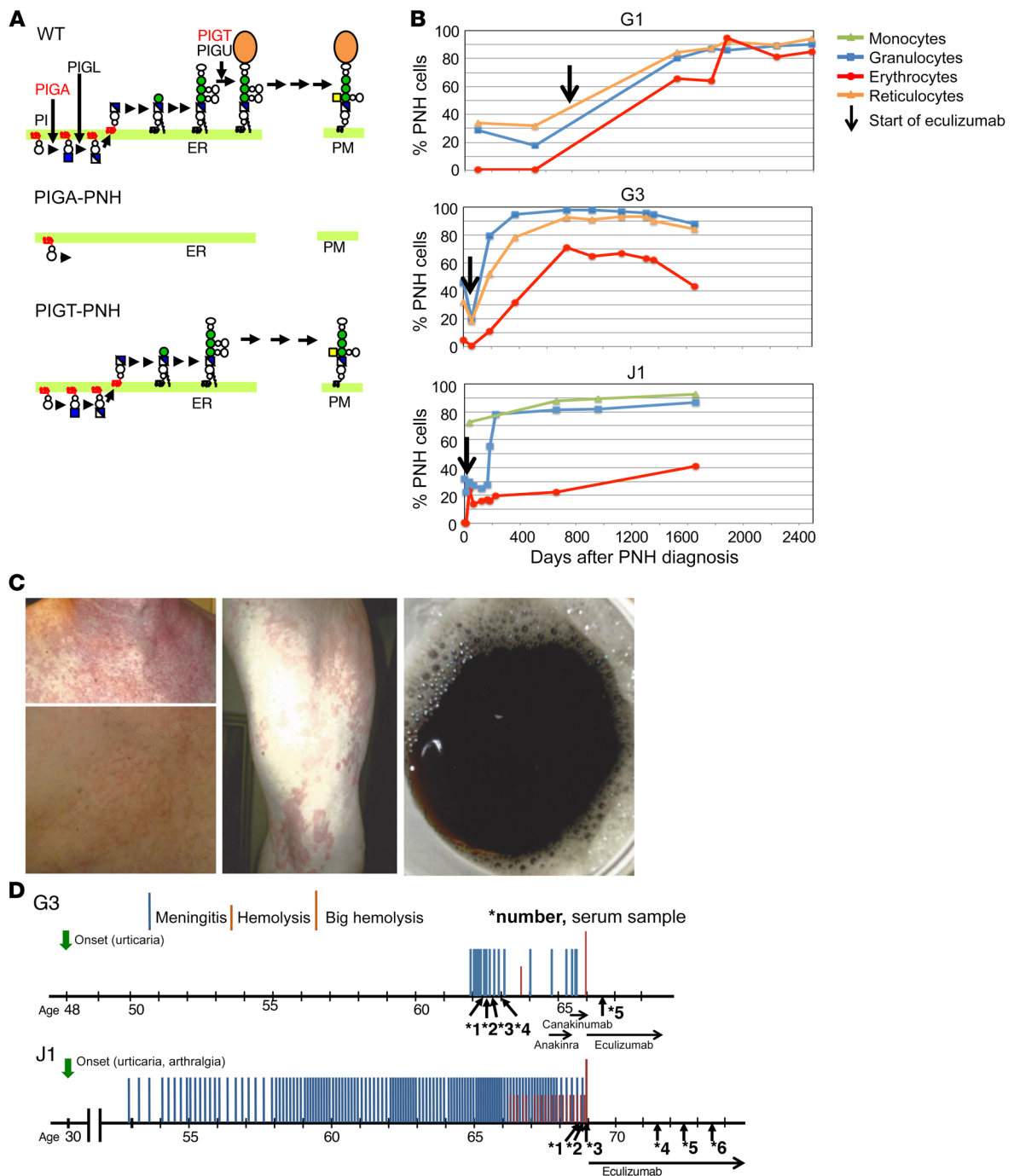


**Figure 1. Clinical features of PIGT-PNH.** (A) Schematics of normal and defective biosynthesis of GPI-APs. (Top) In normal cells, GPI is synthesized in the ER from phosphatidylinositol (PI) by sequential reactions and assembled GPI is attached to proteins (orange oval). PIGA acts in the first step whereas PIGT acts in attachment of GPI to proteins. GPI-APs are transported to the plasma membrane (PM). (Middle) No GPI biosynthesis in PNH caused by *PIGA* defect. (Bottom) Accumulation of free GPI in PNH cells caused by *PIGT* defect. Non-protein-linked GPI is transported to the PM. (B) Time course of PNH clone sizes in patients G1, G3, and J1. Percentages of PNH cells in monocytes, granulocytes, erythrocytes, and reticulocytes are plotted as a function of time in days. Arrows, start of eculizumab therapy. (C) Examples of urticaria in G3 before the start of the anakinra treatment are shown on the left (chest) and middle (left upper leg); hemoglobinuria in G3 is shown on the right. Brightness was adjusted in the bottom chest image to more clearly show raised skin in the affected area. The pictures were made available by the patient. (D) Clinical courses of G3 in comparison to J1 (Figure 1 in ref. 8 was modified with additional data) including effective treatments. G3 (top) had meningitis 19 times between 62–65 years of age. Eculizumab therapy started at 66 years of age after a severe hemolysis. J1 (bottom) had meningitis 121 times between 53–69 years of age when eculizumab therapy started. Downward green arrows, onset of urticaria and/or arthralgia; blue middle height bars, meningitis; orange short bars, hemolysis; orange long bars, severe hemolysis; horizontal arrows of various lengths, treatment periods of effective therapies (anakinra and canakinumab were given with prednisolone); upward arrows with number and asterisk, serum samples taken for cytokine and other protein determination.

**Table 1. Summary of clinical and genetic findings**

	J1 <sup>A</sup>	G1 <sup>B</sup>	G2 <sup>C</sup>	G3 <sup>D</sup>
Age at diagnosis of PNH	68	49	65	66
Sex	Male	Female	Male	Male
Origin	Japanese	White	White	White
Signs and symptoms (age of onset)				
Urticaria	+ (30) <sup>E</sup>	+ (26)		+ (48)
Arthralgia	+ (30)	+ (27)		+ (61)
Myalgia		+ (27)		+ (61)
Aseptic meningitis	+ (53)			+ (61)
Fever	+ (53)			+ (61)
Headache	+ (53)	+ <sup>F</sup>		
Intravascular hemolysis	+ (67)	+ (44) <sup>G</sup>	+	+ (61) <sup>H</sup>
Abdominal pain		+ (39)	+ (61)	
Ulcerative colitis		+ (52) <sup>I</sup>		
Previous therapy	Corticosteroids, colchicine (for symptoms of autoinflammation)	Corticosteroids, diphenhydramine, cromoglycin, azathioprine (for symptoms of autoinflammation)	Corticosteroids (for residual hemolysis after start of eculizumab)	Corticosteroids, mycophenolate mofetil, dapsone, anakinra, canakinumab (for symptoms of autoinflammation)
Eculizumab	+ (69)	+ (52)	+ (66)	+ (66)
M allele of <i>PIGT</i> <sup>J</sup>	c.250G>T <sup>K,L</sup> (p.E84*)	c.1401-2A > G (exon 11 del)	c.761_764delGAAA <sup>M</sup> (p.G254fs)	c.197delA <sup>M</sup> (p.Y66fs)
P allele of <i>PIGT</i> <sup>J</sup>	Entire deletion (18 Mb) <sup>N</sup>	Entire deletion (8 Mb)	Entire deletion (12 Mb) <sup>M,N</sup>	Entire deletion (15 Mb) <sup>M</sup>

<sup>A</sup>J1 had recurrent urticaria and arthralgia since 30 years of age. At 53 years of age, he had first aseptic meningitis and since then had meningitis several times a year. A cerebrospinal fluid sample taken during an episode of meningitis had approximately 2000 polymorphonuclear leukocytes per microliter. Since 58 years of age, frequencies of meningitis increased to twice a month. At 67 years of age, intravascular hemolysis was first noted. His white blood cell counts during the asymptomatic period and after commencement of eculizumab therapy were within a normal range. Refer to ref. 8 for more detailed description of J1. <sup>B</sup>Refer to the Supplemental Data in ref. 7 for detailed description of G1. <sup>C</sup>In G2, 96% of granulocytes and 19% of erythrocytes were GPI-AP-defective. Additional diagnoses and symptoms for G2: arteriosclerosis with coronary heart disease, myocardial infarction (49 years), recurrent left brain transient ischemic attacks (66 years), recurrent confusion symptoms and disturbance of memory; cholecystectomy (43 years) in the years following remission of cholangitis; elevation of indirect bilirubin; B chronic lymphocytic leukemia (64 years), treatment with rituximab (whether leukemic cells were from PNH clone was not known); hemochromatosis (compound heterozygous), diagnosed at age of 66 because of elevation of ferritin, prostate adenoma. The patient died for cardiac decompensation with fulminant pulmonary edema and massive general arteriosclerosis with ulcerated plaques. <sup>D</sup>Additional diagnosis and symptoms for G3: cholelithiasis (65 years); metabolic syndrome with obesity, diabetes, and dyslipoproteinemia; sensorineural hearing loss (61 years); peripheral arterial occlusive disease; JAK2 V617F mutation (age of 66) (whether the mutation occurred in PNH clone was not known), neurinoma left side (52 years), increasing personality changes, and disturbance of memory since the beginning of the meningitis episodes until start of eculizumab. <sup>E</sup>Plus signs indicate presence of corresponding signs and symptoms. Numbers in parentheses indicate age when the symptom was first recognized or eculizumab treatment was started. <sup>F</sup>Headache often occurred associated with urticaria (first urticaria, followed by severe headache). <sup>G</sup>First time of significantly elevated lactate dehydrogenase (LDH) (7). <sup>H</sup>Patient reported dark urine (Figure 1C, right). <sup>I</sup>G1 developed ulcerative colitis/proctitis about 5 years after diagnosis of PNH. Eculizumab was not effective to ulcerative colitis/proctitis in G1. <sup>J</sup>M, maternal; P, paternal. <sup>K</sup>Based on NM\_015937. <sup>L</sup>The same variant c.250G > T in J1 (8) was found in 2 Japanese patients with inherited GPI deficiency (IGD) suffering from developmental delay, seizures, and skeletal abnormality (Supplemental Table 2 and refs. 11, 37). <sup>M</sup>Data are shown in Supplemental Figure 2. <sup>N</sup>Deletions of J1 and G2 included entire *PIGU* gene as well as *PIGT*.

GPI intermediate is generated in *PIGA*-defective cells (Figure 1A, middle). *PIGT* is involved in the attachment of GPI to proteins. GPI is synthesized in the ER, but is not used as a protein anchor in *PIGT*-defective cells (Figure 1A, bottom). We used T5 mAb that recognizes free GPI, but not protein-bound GPI, as a probe to characterize free GPI (Figure 3A and refs. 18, 19; see Methods for epitope and other characteristics of this antibody). Using T5 mAb in Western blotting and flow cytometry, we first compared *PIGT*-defective CHO cells with *PIGL*-defective CHO cells, in which an early GPI biosynthetic step is defective, like in *PIGA*-defective cells. T5 mAb revealed a strong band of free GPI at a position corresponding to approximately 10 kDa in lysates of *PIGT*-defective cells but not of *PIGL*-defective cells (Figure 3B). DAF and CD59 were not detected in either mutant cell, confirming that non-GPI-anchored precursor proteins were degraded (Figure 3B and

ref. 20). T5 mAb stained the surface of *PIGT*-defective CHO cells but not *PIGL*-defective cells, confirming that free GPI transported to the cell surface is detectable by T5 mAb (Figure 3C).

We then analyzed blood cells from J1, G1, and G3, and from patients with *PIGA*-PNH by flow cytometry. All 4 patients had PNH-type blood cells defective in various GPI-APs (Figure 3, D–F, and Supplemental Figure 4, A and B). Erythrocytes from J1, G1, and G3 contained 3%, 84%, and 60% PNH cells, respectively, and a sizable fraction of them (36%, 87%, and 87%, respectively) were stained by T5 mAb (Figure 3D). J1 had PNH cells in granulocytes (81%), monocytes (87%), and B lymphocytes (54%), but not T lymphocytes (<2%), as revealed by anti-CD59 and GPI-binding probe fluorescence-labeled nonlytic aerolysin (FLAER) (21). Affected monocytes and B lymphocytes were strongly stained by T5 mAb, whereas affected granulocytes were weakly but clearly stained (Figure 3E

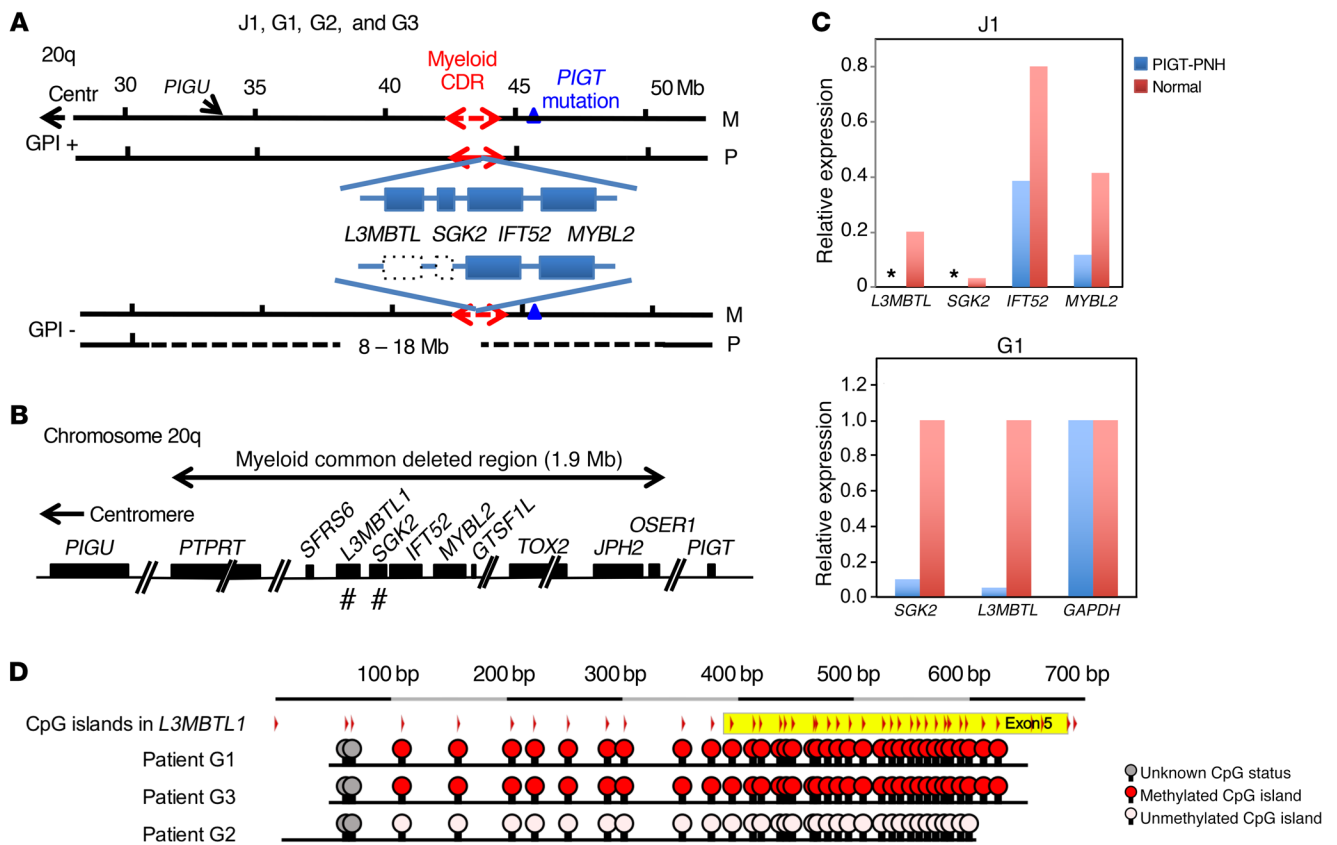


**Figure 2. Genetic abnormalities in patients with PIGT-PNH.** (A) PIGT mutations in GPI-AP-positive (GPI+) and -defective (GPI-) cells from patients with PIGT-PNH. (Top) GPI+ cells from patients J1, G1, G2, and G3 had a germline PIGT mutation (triangle) in the maternal (M) allele. Two maternally imprinted genes, L3MBTL1 and SGK2, within myeloid common deleted region (CDR) are expressed from the paternal (P) allele. Solid and broken red double arrows, P and M alleles of myeloid CDR, respectively. (Bottom) GPI blood cells from PIGT-PNH patients had an 8 Mb to 18 Mb deletion spanning myeloid CDR and PIGT and/or PIGU in the P chromosome 20q leading to losses of expression of L3MBTL1 and SGK2 genes (dotted boxes). (B) A 1.9-Mb region in chromosome 20q spanning PTPRT gene to OSER1 gene is termed myeloid common deleted region. PIGT and PIGU genes are approximately 1.2 Mb telomeric and 7.4 Mb centromeric to the myeloid CDR, respectively. L3MBTL1 and SGK2 genes marked # are maternally imprinted. (C) qRT-PCR analysis of genes within myeloid CDR in GPI-AP-defective granulocytes from J1 and granulocytes from a healthy control (top) and whole blood cells from G1 and a healthy control (bottom). L3MBTL1 and SGK2, maternally imprinted genes; IFT52 and MYBL2, nonimprinted genes. Relative expression is determined taking means of ABL levels as 1 (J1) or of GAPDH as 1 (G1). Blue bars, cells from J1 and G1; orange bars, cells from healthy individuals; \* indicates below detection limits. Mean of duplicate (J1) and triplicate (G1) samples in 1 of the 2 independent experiments. Mean RQ max values for J1 samples were 0.15 (IFT52) and 0.17 (MYBL2), and for normal control samples were 0.034 (L3MBTL1), 0.003 (SGK2), 0.078 (IFT52), and 0.002 (MYBL2). Mean RQ max values for G1 samples were 0.01 (SGK2), 0.004 (L3MBTL1), and 0.01 (GAPDH), and for normal control samples were 0.08 (SGK2), 0.22 (L3MBTL1), and 0.002 (GAPDH). (D) Methylation status of the CpG islands in L3MBTL1 in G1, G2, and G3. Red, methylated CpG islands; pink, unmethylated CpG islands; gray, unknown CpG islands. Bisulfite sequencing data are shown in Supplemental Figure 3A.

and Supplemental Figure 4B). Normal populations in granulocytes, monocytes, and B lymphocytes were not stained by T5 mAb (Figure 3E). Similar results, showing strong T5 staining of affected monocytes and granulocytes, were obtained with leukocytes from G1 and G3 (Figure 3F). In contrast, PNH cells from PIGA-PNH patients and cells from healthy individuals were not positively stained by T5 mAb (Figure 3, E and F). Small fractions of WT erythrocytes from J1, G1, and G3 (0.13%, 9.7%, and 9.5%, respectively) were positively stained by T5 mAb (Figure 3D). Free GPI might be transferred from PNH cells to WT erythrocytes in vivo (22, 23), although the exact mechanism involved needs to be clarified. Thus, the surface expression of the T5 mAb epitope is specific for PIGT-defective cells and T5 mAb is useful to diagnose PIGT-PNH. It was noted that FLAER, which is conveniently used to stain cell-surface GPI-APs and to determine the affected cells in patients with PNH (21, 24), did not

stain PIGT-PNH cells. Aerolysin specifically binds to the GPI moiety of some but not all GPI-APs, and requires simultaneous association with N-glycan for high-affinity binding (25-27). Our results indicate that FLAER binds to protein-bound GPI but not to free GPI.

We next investigated whether GPI-AP-defective clone was present in the stage only with autoinflammation. After determining the break points causing the deletion of 18 Mb in J1 (Supplemental Figure 5), we quantitatively analyzed blood DNA samples for the presence of the break. It was estimated that a relative level of the break in the sample taken in a stage with autoinflammation only (#1) was approximately 10% of a level in the sample taken 1 month after start of eculizumab therapy (#2), which contained 29% PNH cells (Figure 3G). Therefore, approximately 3% of total leukocytes obtained 4 months before the onset of recurrent hemolysis were GPI-AP-defective cells.

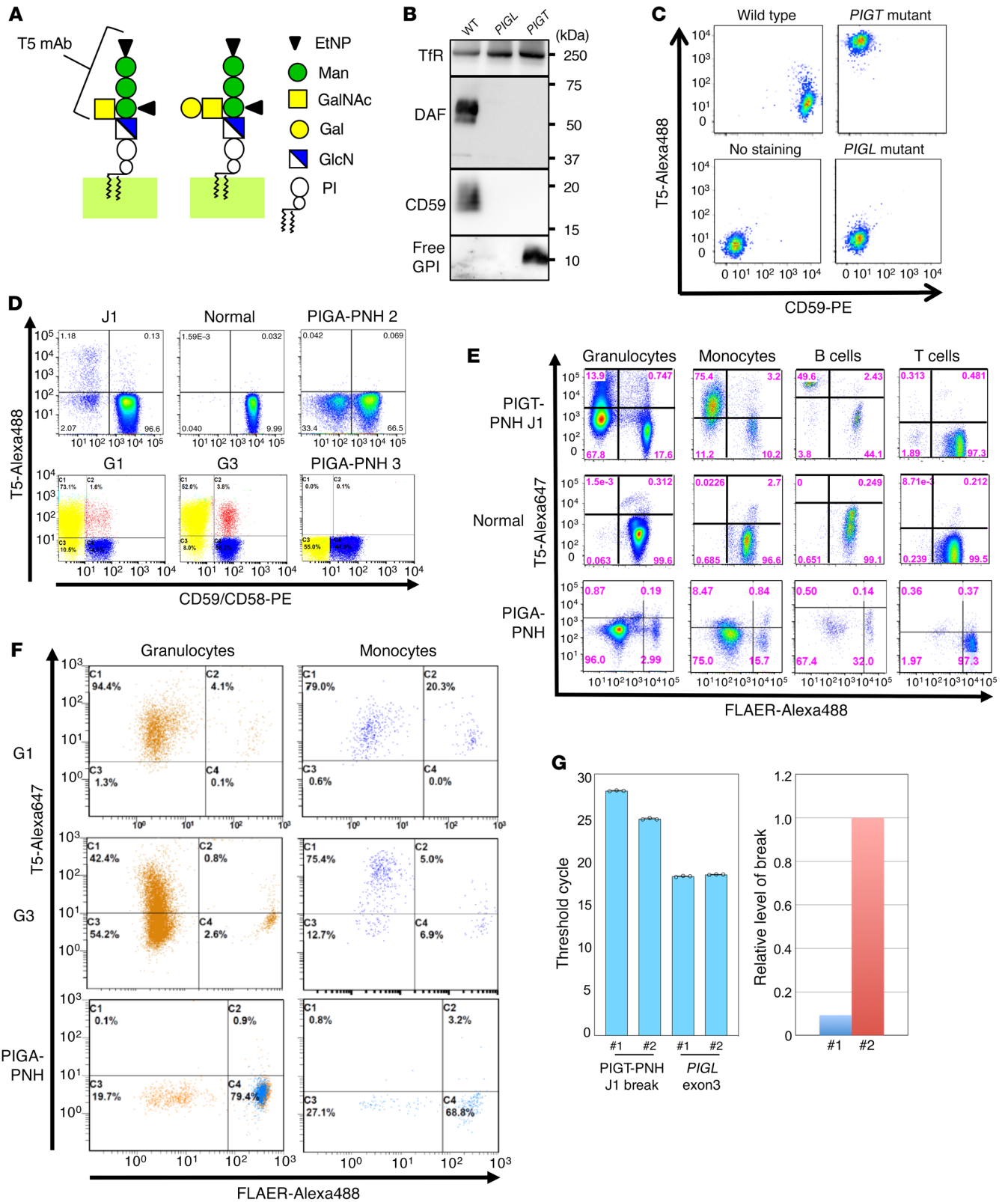


**Figure 3. Biochemical abnormalities in *PIGT*-defective cells.** (A) Schematic representation of binding specificity of T5 mAb. T5 mAb recognizes mammalian free GPI bearing GalNAc-side chain linked to the first mannose (left). T5 mAb does not bind to free GPI when Gal is attached to GalNAc (right). Man, mannose; GlcN, glucosamine; EtNP, ethanolamine phosphate; PI, phosphatidylinositol. (B) Western blotting analysis of *PIGT*-defective and *PIGL*-defective CHO cells with T5 mAb for free GPI, anti-CD59, and anti-DAF mAbs, and anti-transferrin receptor (TfR) as loading controls. (C) Flow cytometry of *PIGT*-defective and *PIGL*-defective CHO cells with T5 mAb and anti-CD59 mAb. (D) Flow cytometry of erythrocytes from J1, G1, G3, a healthy individual, and 2 patients with *PIGA*-PNH with T5 mAb and anti-CD59 (top panels) or anti-CD58 (bottom panels). (E) Flow cytometry of blood cells from J1, a healthy individual, and a patient with *PIGA*-PNH with T5 mAb and FLAER. (F) Granulocytes and monocytes from G1 and G3, and a patient with *PIGA*-PNH, stained by T5 mAb and FLAER. (G) Determination of the PNH clone size in J1 by qPCR analysis of the break causing 18 Mbp deletion. (Left) Threshold cycle in PCR for the break and exon 3 of *PIGL* as a reference. #1, DNA from whole blood leukocytes taken in a stage with autoinflammation only (4 months before the onset of recurrent hemolysis); #2, DNA from granulocytes (29% of cells were GPI-AP-defective) taken 1 month after start of eculizumab therapy. (Right) Relative levels of the break in samples #1 and #2 by setting the level in #2 as 1. Data are shown in mean of triplicate samples in 1 experiment. Mean RQ max values for #1 and #2 samples were 0.092 and 1.11, respectively.

*Inflammasome- and complement-mediated autoinflammation, a feature of *PIGT*-PNH.* IL-18 levels were elevated in serum samples taken from J1 before and after the commencement of eculizumab therapy (Table 2), suggesting that this phenomenon was not dependent upon C5 activation. Serum amyloid A was also elevated before eculizumab therapy, but was within the normal range after the commencement of eculizumab therapy (Table 2), suggesting that the elevation was dependent upon C5 activation. In G3, increased levels of soluble IL-2 receptor and thymidine kinase before, but not after, the start of eculizumab therapy suggested autoinflammation (Table 3). Serum amyloid A (up to 10.5  $\mu\text{g}/\text{mL}$ ; normal range <5  $\mu\text{g}/\text{mL}$ ) was also elevated. Combination therapies of prednisolone with anakinra, an IL-1 receptor antagonist, or canakinumab, a mAb against IL-1 $\beta$ , were effective at reducing urticaria (but not arthralgia and meningitis episodes) of G3. In G1, the IL-18 level was above the normal range during eculizumab therapy (195  $\text{pg}/\text{mL}$ ; normal range <150  $\text{pg}/\text{mL}$ ). These lines of evidence suggest that autoinflammatory symptoms are associated with inflammasome activation. We also measured IL-18, serum amyloid A, and lactate dehydrogenase (LDH) in serum samples from 4 patients with *PIGA*-PNH who were not undergoing eculizumab therapy. The levels of IL-18 (263–443  $\text{pg}/\text{mL}$ ; normal range <211  $\text{pg}/\text{mL}$ ) and serum amyloid A (5.0–8.3  $\mu\text{g}/\text{mL}$ ) were within or slightly higher than the normal ranges, whereas LDH levels were markedly elevated (Table 4). These results suggest that autoinflammation is a feature of *PIGT*-PNH.

We next compared mononuclear cells from J1, patients with *PIGA*-PNH, and healthy donors for IL-1 $\beta$  production upon stimulation by NLRP3-inflammasome activators (28). Cells from 3 *PIGA*-PNH patients secreted only very low levels of IL-1 $\beta$  after stimulation by Pam<sub>3</sub>CSK4 (TLR2 ligand) and ATP or monosodium urate (MSU) (Figure 4A, right, and Figure 4B). In contrast, cells from J1 secreted 45–60 times as much IL-1 $\beta$  and the levels were even higher than those from healthy control cells (Figure 4A, left, and Figure 4B). A similar difference between *PIGT*- and *PIGA*-defective cells was seen upon stimulation by lipoteichoic acid (LTA; another

TLR2 ligand) and ATP or MSU (Figure 4B). Low IL-1 $\beta$  response of *PIGA*-defective cells was predicted because they lack CD14, a GPI-anchored coreceptor of TLRs. However, *PIGT*-defective cells also lacking CD14 showed a strong IL-1 $\beta$  response. These results indicate that NLRP3 inflammasomes are easily activated and support the idea that the presence of non-protein-linked free GPI is associated with efficient activation of NLRP3 inflammasomes, contributing to autoinflammatory symptoms in *PIGT*-PNH.

To investigate the roles of complement in inflammasome activation in *PIGT*-PNH, we switched to a model cell system because patients' blood cells were easily damaged in vitro under conditions of complement activation. *PIGT*-KO and *PIGA*-KO cells were generated from human monocytic THP-1 cells (Supplemental Figure 6A) and were differentiated to macrophages. They showed IL-1 $\beta$  response comparable to those of authentic inflammasome activators (Supplemental Figure 6B). To analyze the inflammasome response to activated complement, these THP-1-derived macrophages were stimulated with acidified serum (AS), which causes activation of the alternative complement pathway. *PIGT*-KO and *PIGA*-KO cells but not WT cells secreted IL-1 $\beta$  (1221.8  $\pm$  91.6  $\text{pg}/\text{mL}$ , 568.2  $\pm$  101  $\text{pg}/\text{mL}$ , and 23.7  $\pm$  2.2  $\text{pg}/\text{mL}$  for *PIGT*-KO, *PIGA*-KO, and WT cells, respectively) (Figure 5A). This result is consistent with impaired complement regulatory activities on *PIGT*-KO and *PIGA*-KO cells, and normal complement regulatory activity on WT cells. *PIGT*-KO cells secreted approximately twice as much IL-1 $\beta$  as *PIGA*-KO cells ( $P < 0.01$ ). However, IL-1 $\beta$  production returned to near the WT cell level after the transfection of *PIGT* and *PIGA* cDNAs into *PIGT*-KO and *PIGA*-KO cells, respectively (Figure 5B). The levels of IL-1 $\beta$  mRNA and protein were comparable in WT, *PIGT*-KO, and *PIGA*-KO cells (Supplemental Figure 7, A and B). Therefore, knock out of *PIGT* enhanced the secretion but not the generation of IL-1 $\beta$ .

Heat inactivation of complement and the addition of anti-C5 mAb to AS almost completely inhibited IL-1 $\beta$  secretion (Figure 5A). These results indicate that IL-1 $\beta$  secretion requires the activation of C5 on *PIGT*-KO and *PIGA*-KO cells. The activation of C5 leads to 2 biologically active products, C5a and MAC (29). To address which of these is important for IL-1 $\beta$  secretion, cells were treated with the C5aR antagonist W-54011 (30) or anti-C5aR mAb to inhibit the signal transduction through C5aR. WT, *PIGT*-KO, and *PIGA*-KO cells expressed C5aR at similar levels (Supplemental Figure 7C). The 2 methods of functional inhibition of C5aR had little effect on IL-1 $\beta$  secretion, indicating that the signal through C5aR plays no major role in this cell system (Figure 5C). Next, AS-treated cells were analyzed for surface binding of C3b fragments and MAC. Exposure to AS resulted in the higher binding of C3b fragments and MAC on *PIGT*-KO cells compared with that on *PIGA*-KO cells (Figure 5D and Supplemental Figure 8, A and B). The level of MAC was several times higher on *PIGT*-KO cells than on *PIGA*-KO cells, suggesting that complement activation was enhanced, leading to the enhanced formation of MAC on *PIGT*-KO cells. To confirm the role of MAC in IL-1 $\beta$  secretion, *PIGT*-KO cells were treated with acidified C6- and C7-depleted sera, in which C5a generation is intact whereas MAC formation is impaired. IL-1 $\beta$  secretion was greatly reduced by C6 or C7 depletion and was restored by the replenishment of C6 or C7 (Figure 5E). These results suggest that MAC but not C5a plays a critical

**Table 2. J1: cytokines and other proteins in serum samples**

Serum samples <sup>A</sup>	*1, interval	*2, meningitis	*3, hemolysis	*4, 2.5 years after start of eculizumab	*5, 3.5 years after start of eculizumab	*6, 4.5 years after start of eculizumab	Normal range
IL-18 (pg/mL)			1410	797	972	1150	<211.0
IL-1 $\beta$ (pg/mL)	0.291	<0.125	4.670	<0.125	<0.125	<0.125	<0.928
IL-1RA (pg/mL)	716	323	27500	239			85.6–660
IL-6 (pg/mL)		127.0	4160	2.30	2.94	6.32	<2.410
Serum amyloid A ( $\mu$ g/mL)	175.8	2433.0	282.6	<2.5			<8.0
LDH (IU/L)	291	249	3004	157	165	169	120–250

IL-1RA, IL-1 receptor antagonist. <sup>A</sup>Serum samples correspond to asterisked numerals in Figure 1D, representing samples from patient J1 during the indicated health events.

role in the secretion of IL-1 $\beta$ . It is also suggested that free GPI plays some role in complement activation, leading to the enhanced binding of C3b fragments and MAC formation.

To determine whether the structure of free GPI (presence or absence of Gal capping) affects complement activation and subsequent IL-1 $\beta$  secretion, we knocked out *SLC35A2* in *PIGT*-KO THP-1 cells. *PIGT*-*SLC35A2* double-KO THP-1 cells were strongly stained by T5 mAb as expected (Supplemental Figure 6C). The binding of both C3b fragments and MAC increased approximately 5 times after *SLC35A2* KO (Figure 5F). Concomitantly, the secretion of IL-1 $\beta$  more than doubled (Figure 5G). These results indicate that the structure of free GPI influenced complement activation efficiency and subsequent IL-1 $\beta$  secretion.

Finally, we asked whether only the alternative pathway is involved in binding of C3b fragments on *PIGT*-KO and *PIGA*-KO THP-1 cells, or the lectin and/or the classical pathway is also involved. For this, cells were stained with anti-C4d mAb after treatment with acidified serum because activation of either pathway would result in binding of C4b, which is in turn converted to C4d (31, 32). C4d fragments were bound on *PIGT*-KO cells and the binding was inhibited by 100 mM mannose by approximately 50% but not by *N*-acetylglucosamine (Figure 5H, top, and Supplemental Figure 8D). Binding of C3b fragments on *PIGT*-KO cells was also inhibited by mannose by approximately 60% but not by *N*-acetylglucosamine (Figure 5H, bottom). These results suggest that the lectin pathway was activated on *PIGT*-KO THP-1 cells, accounting for at least 60% of C3b fragments. C4d fragments were bound on *PIGA*-KO cells at lower levels (60%–70% of *PIGT*-KO cell levels), which were not inhibited by either *N*-acetylglucosamine or mannose. Mannose, but not *N*-acetylglucosamine, mildly inhibited binding of C3b fragments on *PIGA*-KO cells (Figure 5H). It is unclear at the moment whether the classical pathway was

involved in residual C4d binding on *PIGT*-KO cells in the presence of 100 mM mannose or in C4d binding on *PIGA*-KO cells.

## Discussion

We studied patients with PNH caused by *PIGT* mutations. Because PNH caused by *PIGT* mutations is characterized by auto-inflammatory symptoms, we propose that they represent a new disease entity, *PIGT*-PNH. Patients with *PIGT*-PNH had a germline heterozygous mutation in the *PIGT* gene in combination with somatic deletion of the normal *PIGT* gene. Germline *PIGT* mutations were reported in patients with inherited GPI deficiency (IGD) (Supplemental Table 2), which is characterized by developmental delay, seizures, hypotonia, and typical facial dysmorphism (11, 33–39). Inflammatory symptoms and intravascular hemolysis were not reported in IGD patients with *PIGT* mutations. They had either partial loss-of-function homozygous mutations, or combinations of a partial loss-of-function mutation and a null or nearly null mutation. Therefore, cells from the patients with IGD have only partially reduced *PIGT* activities and express only partially reduced levels of CD59 and DAF/CD55, and may have free GPI only to a small extent. In contrast, both germline and somatic mutants in *PIGT*-PNH were functionally null or nearly null (Table 1). Therefore, the affected cells from *PIGT*-PNH patients lost CD59 and DAF/CD55 severely or completely and had high levels of free GPI. Interestingly, the same mutation c.250G>T (p.E84X) was found in J1 and 2 Japanese patients with IGD (11, 37) who were not related to each other. *PIGT*-PNH patient J1 and the mothers of 2 IGD patients from families 2 and 7 had the same heterozygous nonsense *PIGT* mutation (Table 1 and Supplemental Table 2). These mothers were healthy and no inflammatory symptoms were reported for them (11, 37), suggesting that autoinflammation of J1 was not caused by haploinsufficiency of *PIGT* but was initiat-

**Table 3. G3: cytokines and other proteins in serum samples**

Serum samples <sup>A</sup>	*1, meningitis	*2, meningitis	*3, meningitis	*4, meningitis	*5, six months after start of eculizumab	Normal range
Thymidine kinase (U/L)	101	33.6	43.8	Not done	Normal	<5
Soluble IL-2 receptor (U/mL)	1750	1345	3026	1237	Normal	158–635

<sup>A</sup>Serum samples correspond to asterisked numerals in Figure 1D, representing samples from patient G3 during the indicated health events.

**Table 4. PIGA-PNH: cytokines and other proteins in serum samples**

Patient	1	2	3	4	Normal range
IL-18 (pg/mL)	288	289	263	443	<211.0
Serum amyloid A (μg/mL)	5.0	7.1	6.8	8.3	<8.0
LDH (IU/L)	633	1190	923	1216	103-229

Data for 4 patients without eculizumab therapy.

ed after the somatic loss of the other *PIGT* copy occurred. Inheritance of the germline *PIGT* mutations in PIGT-PNH patients is not formally proven because DNA samples were not available from their families. A reported allele frequency of the germline variant *PIGT* of J1 and 2 Japanese families of IGD, c.250G>T (p.E84X), is 0.0002316 in the East Asian population, suggesting that 55,000

Japanese may have this variant (40). It is, therefore, highly likely that J1 inherited the *PIGT* variant.

The expansion of *PIGA*-defective clones in PNH is caused by selective survival under autoimmune bone marrow failure in most cases (41-43). This mechanism was first formulated by Rotoli and Luzzatto in 1989 (41). In few cases, clonal PNH cells acquired benign tumor characteristics by additional somatic mutations (44-46). In contrast, none of the patients with PIGT-PNH had documented bone

marrow failure (Supplemental Figure 1A and refs. 7, 8). In addition, the myeloid CDR is lost in *PIGT*-defective clones in PIGT-PNH, similar to the case in clonal cells in myeloproliferative 20q<sup>-</sup> syndromes. The causal relationship between the myeloid CDR loss in PIGT-PNH and clonal expansion needs to be proven, particularly because boosted lineages under L3MBTL1 and SGK2 loss differ

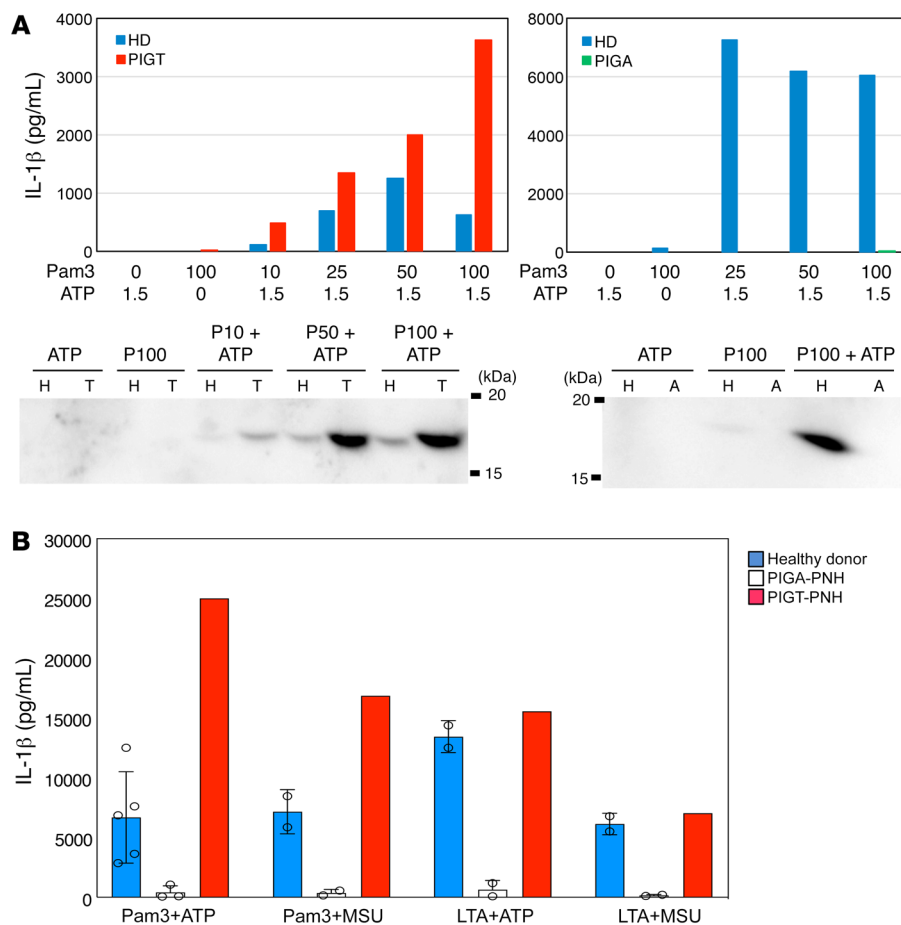


**Figure 4. IL-1β secretion from PIGT-PNH and PIGA-PNH cells.** (A) The peripheral blood mononuclear cells from J1, PIGA-PNH4, and a healthy individual were incubated with 10-100 ng/mL Pam<sub>3</sub>CSK4 (Pam3) at 37°C for 4 hours, and then were incubated with 1.5 mM ATP for 30 minutes. IL-1β in the supernatants was measured by ELISA (top) and Western blotting (bottom). (Left) J1 (red bars) and a healthy individual (blue bars). (Right) PIGA-PNH4 (green bars) and a healthy individual (blue bars). P10, P50, and P100, 10, 50, and 100 ng/mL Pam<sub>3</sub>CSK4, respectively; H, healthy donors; T, PIGT-PNH; A, PIGA-PNH. (B) The peripheral blood mononuclear cells from J1, 2 or 3 patients with PIGA-PNH, and 2 or 5 healthy controls were stimulated with 200 ng/mL of Pam3 or 1 μg/mL of lipoteichoic acid (LTA) from *Staphylococcus aureus* for 4 hours at 37°C, and after washing were incubated with 3 mM ATP or 200 μg/mL monosodium ureate (MSU) for 4 hours at 37°C. IL-1β secreted into the medium was determined by ELISA. Data for healthy donors and PIGA-PNH were shown as mean ± SD. Cells from 3 patients with PIGA-PNH (PIGA-PNH4-6) secreted very low levels of IL-1β (403 ± 326 pg/mL) after stimulation of NLRP3-inflammasomes with Pam<sub>3</sub>CSK4 and ATP under these strong conditions. In contrast, cells from PIGT-PNH J1 secreted IL-1β at a high level (25,000 pg/mL), a level that is higher than those from 3 healthy donors (6693 ± 1711 pg/mL). Similar results were obtained by stimulation with Pam<sub>3</sub>CSK4 and MSU instead of ATP. Moreover, similar results were obtained by stimulation with LTA plus ATP or MSU.

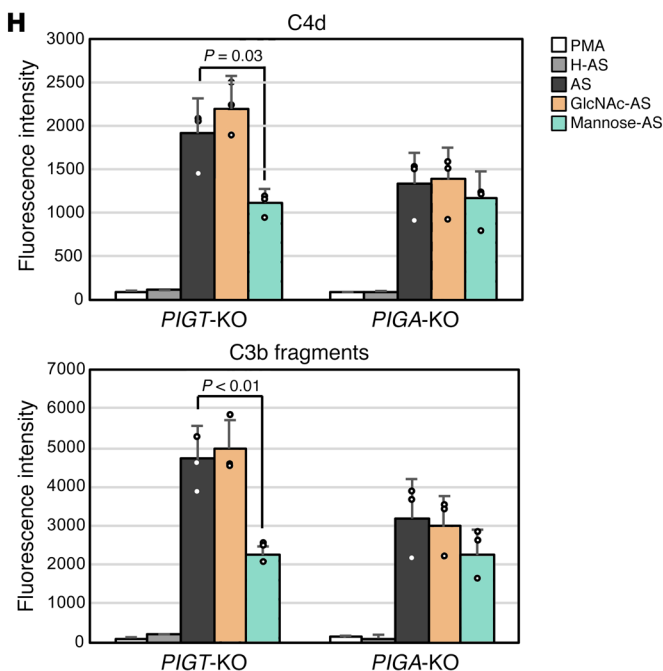
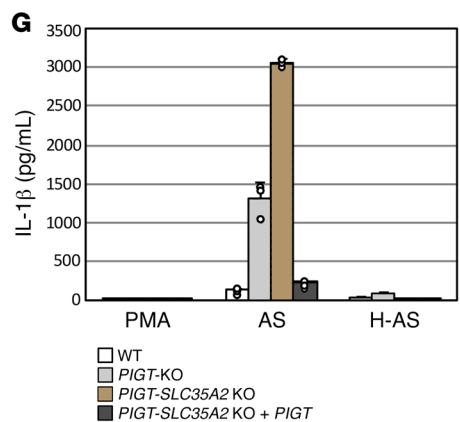
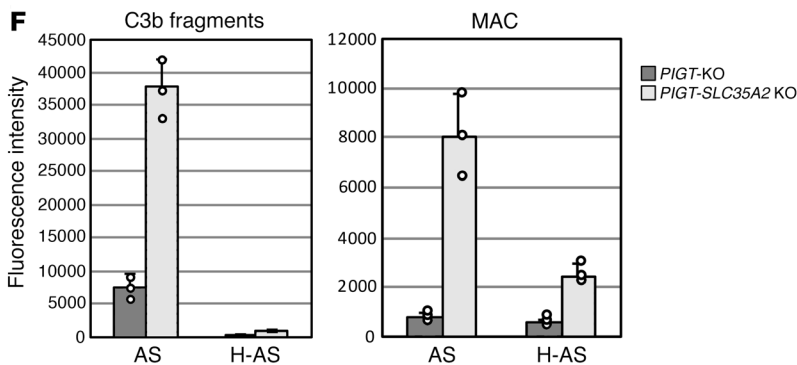
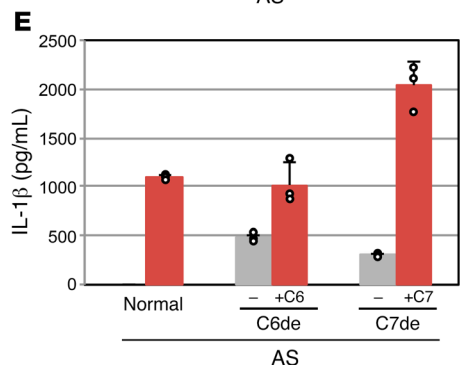
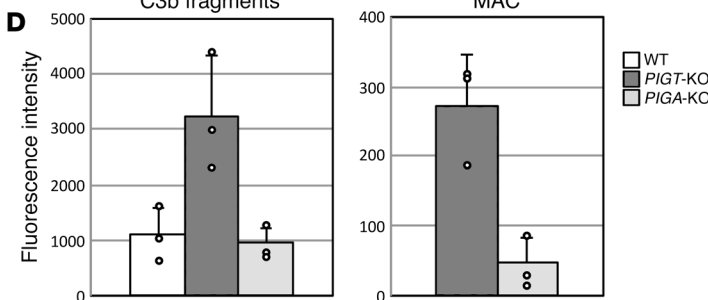
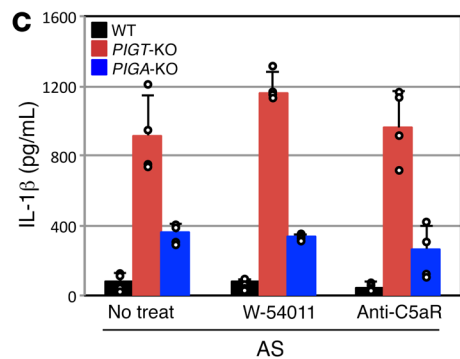
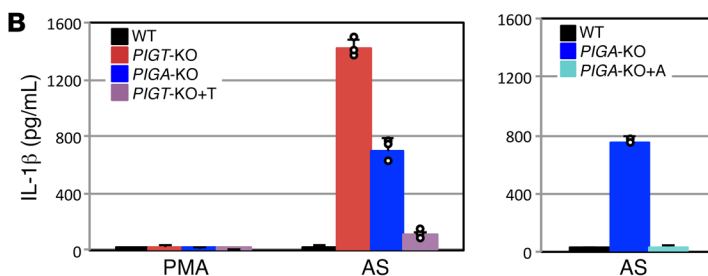
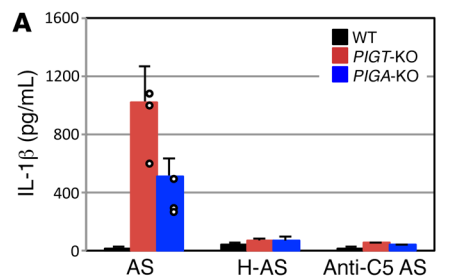


**Figure 5. IL-1 $\beta$  secretion from and binding of complement components to PIGT- and PIGA-defective THP-1 cells.** (A) Complement-mediated IL-1 $\beta$  secretion from THP-1-derived macrophages. WT, *PIGT*-KO, and *PIGA*-KO cells were incubated with acidified serum (AS), heat-inactivated AS (H-AS), or AS containing anti-C5 mAb. Supernatant samples were collected after a 5-hour incubation and analyzed for IL-1 $\beta$  by ELISA. Mean  $\pm$  SD of 3 independent experiments. (B) Reductions of IL-1 $\beta$  secretion by transfection of *PIGT* and *PIGA* cDNAs into *PIGT*-KO and *PIGA*-KO cells (*PIGT*-KO+T and *PIGA*-KO+A, respectively). Cells differentiated by PMA were either left untreated (PMA) or incubated with AS (AS) under similar conditions as described in A, and supernatants analyzed for IL-1 $\beta$ . Mean  $\pm$  SD of 3 independent experiments. (C) Effect of inhibiting C5aR on IL-1 $\beta$  secretion from THP-1-derived macrophages. Cells were incubated with AS alone (no treat), or AS containing C5aR antagonist (W-54011) or anti-C5aR mAb. Supernatant was collected after 5 hours and analyzed for IL-1 $\beta$  by ELISA. Mean  $\pm$  SD of duplicate samples from 2 independent experiments. (D) Detection of C3b fragments (left) and MAC (right) by flow cytometry on PMA-differentiated THP-1 macrophages after incubation with AS. Geometric mean fluorescence intensity of medium-treated cells was subtracted from that of AS-treated cells. Mean  $\pm$  SD of 3 independent experiments. (E) IL-1 $\beta$  secretion from *PIGT*-KO THP-1 macrophages stimulated with C6- or C7-depleted AS. *PIGT*-KO THP-1 macrophages were incubated with AS, C6-depleted AS (-/C6de), C6de restored by C6 (+C6/C6de), C7-depleted AS (-/C7de), or C7de restored by C7 (+C7/C7de). Supernatant was collected after overnight incubation. Mean  $\pm$  SD of triplicate samples from 2 independent experiments (normal and C6-depleted sera) and 1 experiment (C7-depleted serum). (F) Binding of C3b fragments (left) and MAC (right) on *PIGT*-KO and *PIGT*-*SLC35A2* double KO THP-1 macrophages after AS treatments. (G) IL-1 $\beta$  secretion from *PIGT*-KO and *PIGT*-*SLC35A2* double KO THP-1 macrophages after AS treatments. (H) Bindings of C4d (top) and C3b fragments (bottom) on *PIGT*-KO and *PIGA*-KO THP-1 macrophages after AS treatments and inhibition by mannose. Two-tailed Student's *t* test was used for analysis. Mean  $\pm$  SD of 3 independent experiments.

between in vitro study (13) and *PIGT*-PNH patients, and because platelet and leukocyte counts were not much changed in *PIGT*-PNH patients (Supplemental Figure 1A). Complement dysregulation, which is present in *PIGT*-PNH but not in myeloproliferative 20q- syndromes, might modulate blood cell profiles. Nevertheless, this unique deletion occurs in *PIGT*-PNH but not in *PIGA*-PNH. Taking these findings together, it is likely that the mechanism of clonal expansion for *PIGT*-PNH is distinct from that for *PIGA*-PNH cells (see models in Supplemental Figure 3B).

Whereas *PIGT*-PNH shares intravascular hemolysis and thrombosis with PNH, *PIGT*-PNH is characterized by autoinflammatory symptoms including recurrent urticaria, arthralgia, and aseptic meningitis. *PIGT*-PNH first manifested with autoinflammatory symptoms alone and symptoms of PNH became apparent many years later (Table 1). It is possible that different clinical symptoms appear depending on the size of the *PIGT*-defective clone. When the clone size is small, autoinflammation but not PNH may occur and, when the clone size becomes sufficiently large, PNH may become apparent. The idea that the *PIGT*-defective clone is small when only autoinflammation is seen was supported by analyzing J1 DNA obtained before the start of recurrent hemolysis, only approximately 3% of total leukocytes being *PIGT*-defective (Figure 3G). Inflammatory symptoms, recurrent urticaria, arthralgia, fever, and especially meningitis seen in *PIGT*-PNH are shared by children with cryopyrinopathies or cryopyrin-associated periodic syndrome (reviewed by Neven et al, ref. 47). Cryopyrinopathies are caused by gain-of-function mutation in *NLRP3* that leads

to easy activation of *NLRP3* inflammasomes in monocytes and autoinflammatory symptoms (47), further suggesting that inflammasomes are activated in monocytes from *PIGT*-PNH patients. It was reported that autoinflammation occurs in patients having mosaicism with *NLRP3*-mutant cells even when the mutant clone size is small (frequency of mutant allele in whole-blood cells being 4.3% to 6.5%) (48). This is relevant to the symptoms/clone size relationship in *PIGT*-PNH as discussed above.

C5 activation must be involved in the autoinflammatory symptoms in *PIGT*-PNH because they were suppressed by eculizumab. It is important to consider GPI-AP deficiency for patients with recurrent autoinflammatory symptoms such as aseptic meningitis even when PNH symptoms are absent because eculizumab may be effective for such cases. Because DAF and CD59 are missing on *PIGT*-defective monocytes, C5a and MAC might be generated once complement activation has been initiated. It was reported that subarachnoidal application of C5a in rabbits and rats induced acute experimental meningitis (49). Various types of myeloid cells are present in the central nervous system (reviewed in ref. 50). If C5 activation occurs on some of those cells lacking complement regulatory function and C5a is generated, aseptic meningitis might ensue.

The involvement of complement in inflammasome activation has been shown in various blood cell systems (51–54). Indeed, in the THP-1 cell model system, IL-1 $\beta$  secretion was induced by complement in both *PIGT*-KO and *PIGA*-KO cells and more strongly in *PIGT*-KO cells, mainly through MAC formation (Figure 5, A, B, and E). *PIGT*-PNH mononuclear cells were activated by conventional stimulators of inflammasomes similar to or even stronger than healthy control cells. Because blood mononuclear cells were easily lysed by acidified serum, the effect of complement on inflammasome activation in mononuclear cells could not be addressed. Taking the obtained findings together with the results for THP-1 cells, we speculate that *PIGT*-deficient monocytes show an enhanced inflammasome response when complement is activated. How free GPI is involved in inflammasome and complement activation needs to be further clarified to fully understand the mechanistic basis of *PIGT*-PNH.

*PIGU* is an essential component of GPI transamidase, forming a protein complex with *PIGT*, *PIGS*, *PIGK*, and *GPAA1* (Figure 1A and ref. 55). *PIGU*-defective cells do not express GPI-APs on their surface (55). The *PIGU* gene is localized at approximately 7.4 Mb centromeric to the myeloid CDR (Figure 2, A and B), and regions of somatic deletions of 18 Mb and 12 Mb in GPI-AP-defective cells from J1 and G2, respectively, included the entire *PIGU* gene as well as myeloid CDR and *PIGT* gene. The levels of *PIGU* protein in these cells would be around half of the normal levels. It appears unlikely that the 50% reduction in *PIGU* has a significant impact on these cells. The levels of *PIGT* protein in the same cells would be zero or very low because mutations in the remaining *PIGT* gene are a nonsense mutation (E84X) in J1 and a frameshift mutation (frameshift after G254) in G2. For any remaining *PIGT* protein, half of the normal amounts of *PIGU* protein would be excessive for making the GPI transamidase complex. However, it is conceivable that, if a similar somatic deletion including *PIGU* and myeloid CDR occurs in a hematopoietic stem cell of an individual who bears a germline *PIGU* loss-of-function mutation, PNH with autoinflammation caused by *PIGU* mutation might occur.

Eculizumab was used for patients with PIGT-PNH. There are similarities and differences between PIGT-PNH and PNH against treatments with eculizumab. Similar to PNH, eculizumab was effective in preventing intravascular hemolysis in PIGT-PNH. Also similar to PNH, eculizumab caused appearance of direct Coombs-positive erythrocytes in patient G1, suggesting an induction of extravascular hemolysis (7). Patient G2 had residual hemolysis after start of eculizumab therapy, also suggesting extravascular hemolysis (Table 1). *PIGT*-KO THP-1 cells accumulated higher levels of C3b fragments upon complement activation (Figure 5D) and the affected erythrocytes from PIGT-PNH patients express free GPI (Figure 3D). Whether the free GPI-bearing PNH erythrocytes from PIGT-PNH patients accumulate more C3b fragments than PNH erythrocytes from *PIGA*-PNH patients and hence are more prone to extravascular hemolysis is yet to be clarified.

A difference is that percentage of PIGT-PNH cells increased not only in erythrocytes but also in granulocytes after treatment with eculizumab (Figure 1B). It is well known that percentage of PNH erythrocytes increases after eculizumab treatment because intravascular destruction of PNH erythrocytes is prevented by eculizumab (4). However, a sharp increase in percentage of PNH granulocytes seen in G1, G3, and J1 has not been reported in *PIGA*-PNH (4). A possible explanation for the difference is that PIGT-PNH granulocytes might have been destroyed in the blood by complement-dependent mechanisms. MAC formation was much higher on *PIGT*-KO THP-1 cells than on *PIGA*-KO cells (Figure 5D). If levels of MAC formation on *PIGT*-defective granulocytes are similarly high, MAC-mediated cell lysis might occur and eculizumab might prevent it, leading to an increase in the percentage of PNH granulocytes. Another possibility is that the commencement of eculizumab treatment was only coincident with the active phase of clonal expansion. Because hemolysis becomes apparent only when clone size has increased, it is still possible that use of eculizumab is not causally related to increase of PNH granulocytes but that eculizumab treatment was done during active clonal expansion.

Eculizumab was effective in preventing recurrent autoinflammatory symptoms of PIGT-PNH. After start of eculizumab therapy, aseptic meningitis has not occurred in patients G3 and J1, and other symptoms such as urticaria and arthralgia were also prevented (Figure 1D and ref. 8). These autoinflammatory symptoms, therefore, are dependent upon C5 activation. Results with *PIGT*-KO THP-1 cells indicated that IL-1 $\beta$  secretion after complement activation was mediated by MAC rather than C5a (Figure 5, C and E). Patient J1 had elevated levels of IL-18 and serum amyloid A (Table 2). After start of eculizumab, serum amyloid A level turned normal whereas IL-18 levels remained 4–5 times of the upper limit of normal. IL-18 secretion in PIGT-PNH, therefore, is not dependent upon terminal complement activation. C3 activation on the surface of *PIGT*-defective cells was higher than that on *PIGA*-defective cells, as suggested by experimental results with *PIGT*-KO and *PIGA*-KO THP-1 cells (Figure 5, D and E). It appeared that the activation of the lectin pathway was enhanced, leading to elevated levels of C3b fragment binding and MAC formation (Figure 5, D and H). The C4d binding on *PIGT*-KO cells was significantly inhibited by mannose, suggesting that recognition of mannose residues in free GPIs by complement lectins might be involved in the lectin pathway activation. It seems likely that enhanced

C3 activation is involved in the elevation of serum IL-18 levels because C3 activation continues on *PIGT*-defective cell-surface during eculizumab therapy. Causal relationship between free GPIs and C3 activation, and the molecular mechanisms involved, needs to be clarified to know whether earlier steps in complement activation are involved in pathogenesis of PIGT-PNH.

## Methods

**Blood samples and flow cytometry.** Peripheral blood samples were obtained from patients J1 (8), G1 (7), G2, and G3 with PIGT-PNH, and 6 patients with PNH after written informed consent. Peripheral blood leukocytes (Supplemental Figure 1B), erythrocytes, and reticulocytes were stained for GPI-APs by FLAER (Cederlane), anti-CD14 (clone MOP9, BD Biosciences), anti-CD16 (clone 3G8, BioLegend), anti-CD24 (clone ML5, BioLegend), anti-CD48 (BJ40, BioLegend), anti-CD59 (clone 5H8) (56), or anti-CD66b (clone 80H3, Beckman Coulter Immunotech). T5-4E10 mAb (T5 mAb) against free GPI of *Toxoplasma gondii* was a gift from J. F. Dubremetz (18). T5 mAb is now available from BEI Resources, NIAID, NIH (Bethesda, MD). T5 mAb recognizes mammalian free GPI bearing *N*-acetylgalactosamine (GalNAc) side-chain linked to the first mannose (Figure 3A and ref. 19). T5 mAb does not bind to free GPI when galactose (Gal) is attached to GalNAc. Therefore, reactivity of T5 mAb to free GPI is affected by an expression level of Gal transferase that attaches Gal to the GalNAc. Other antibodies used were PE-anti-CD55/DAF (clone IA10, BD Biosciences), PE-anti-CD88/C5aR (BioLegend), and anti-TfR (clone H68.4, Thermo Fisher Scientific). Cells were analyzed by a flow cytometer (MACSQuant Analyzer VYB or FACSCalibur) and FlowJo software.

**DNA and RNA analyses.** Granulocytes with PNH phenotype were separated from normal granulocytes by cell sorting after staining by FLAER. DNA was analyzed for mutations in genes involved in GPI-AP biosynthesis by target exome sequencing, followed by confirmation by Sanger sequencing (7). DNA was also analyzed by array comparative genomic hybridization for deletion (7). Methylation status of CpG was determined by bisulfite sequencing and a SNUPE assay (13). Total RNA was extracted with the RNeasy Mini Kit (Qiagen) including DNase digestion and DNA cleanup, and reverse transcription was performed with the SuperScript VILO cDNA Synthesis Kit (Invitrogen). Levels of *L3MBTL1*, *SGK2*, *IFT52*, *MYBL2*, *ABL*, and *GAPDH* mRNAs were analyzed by quantitative real-time PCR (Supplemental Table 1).

**Cell lines.** *PIGT*-defective CHO cells and *PIGL*-defective CHO cells were reported previously (11, 57). CRISPR/Cas9 system was used to generate *PIGT*-KO and *PIGA*-KO human monocytic THP-1 cells (ATCC) (Supplemental Table 1 for guide RNA sequences). Knockout cells were FACS sorted for GPI-AP-negative cells. Each knockout cell was rescued by transfection of a corresponding cDNA. *SLC35A2* gene was knocked out in *PIGT*-KO THP-1 cells by CRISPR/Cas9 system.

**Inflammasome activation and IL-1 $\beta$  measurements.** Toll-like receptor 2 (TLR2) ligands Pam<sub>3</sub>CSK4 and *Staphylococcus aureus* LTA are from InvivoGen (28, 58). ATP and MSU for activating inflammasomes are from Enzo Life Sciences and InvivoGen (28, 59). Peripheral blood mononuclear cells were stimulated by Pam<sub>3</sub>CSK4 or LTA for 4 hours at 37°C and after washing by ATP or MSU for 4 hours at 37°C. IL-1 $\beta$  ELISA kit (BioLegend) was used to measure IL-1 $\beta$  secreted into the supernatants. Polyclonal rabbit anti-IL-1 $\beta$  antibody for Western blotting was from Cell Signaling Technology. *PIGA*-KO, *PIGT*-KO, and WT THP-1 cells were differentiated into adherent macrophages in complete RPMI

1640 medium containing 100 ng/mL phorbol 12-myristate 13-acetate (PMA; InvivoGen) for 3 hours, and then with fresh complete medium overnight (60). For stimulation, medium was replaced with serum-free medium with Pam<sub>3</sub>CSK<sub>4</sub> (200 ng/mL), followed 4 hours later by ATP stimulation for 4 hours (5 mM).

**Stimulation of THP-1-derived macrophages with complement.** As a source of complement, whole blood was collected from healthy donors after written informed consent, and serum separated, aliquoted, and stored at -80°C prior to use. Inactivation of complement was carried out by heating serum at 56°C for 30 minutes. To prepare AS that allows activation of the alternative pathway on the cell surface, 21 volumes of serum was mixed with 1 volume of 0.4M HCl to have a pH of approximately 6.7. C6- and C7-depleted sera and purified C6 and C7 proteins were purchased from Complement Technology. Differentiated cells were stimulated with acidified normal serum, or acidified C6-depleted and C7-depleted sera, and those reconstituted with C6 and C7, respectively, at 37°C for 5 hours, and secreted IL-1β was measured by ELISA. C5 was inhibited by addition of 35 μg/mL anti-C5 mAb (eculizumab, Alexion Pharmaceuticals).

For ex vivo blockade of human C5aR, anti-human C5aR or nonpeptide C5aR antagonist W-54011 (5 μM, Merck Millipore) (30) was used. Complement C3 and C4 fragments and MAC deposited on the cells were measured by flow cytometry. THP-1 cells were suspended in 20 μl FACS buffer (PBS, 1% BSA, 0.05% sodium azide) with 1:20 human TruStain FcX (Fc receptor blocking solution) at room temperature for 10 minutes. Cells were stained with anti-C3/C3b/iC3b/C3d mAb (clone 1H8, BioLegend), anti-C4d mAb (clone 12D11, Hycult Biotech) or rabbit anti-human SC5b-9 (MAC) polyclonal antibodies (Complement Technology) in FACS buffer. After washing twice, cells were incubated with the PE-conjugated goat anti-mouse IgG (BioLegend) or Alexa Fluor488-conjugated goat anti-rabbit IgG (Thermo Fisher Scientific) secondary antibody. The anti-human SC5b-9 polyclonal antibodies positively stained PMA-differentiated THP-1 cells without incubation in AS. The same antibodies did not stain similarly differentiated *PIGT*-KO and *PIGA*-KO THP-1 cells, suggesting that the antibody product contained antibodies reacted with some GPI-AP expressed on THP-1-derived macrophages (Supplemental Figure 8, B and C). Because of this reactivity to non-MAC antigen(s), the anti-SC5b-9 antibodies were used for *PIGT*-KO and *PIGA*-KO cells but not for WT cells in experiments shown in Figure 5, D and F. To inhibit the lectin pathway, serum was mixed with mannose or *N*-acetylglucosamine (final concentration of 100 mM) before acidification (61).

**Statistical analyses.** All experiments with THP-1 cells were performed at least 3 times. All values were expressed as the mean ± SD of individual samples. For 2-group comparisons between *PIGT*-KO and *PIGA*-KO cells, 2-tailed Student's *t* test was used. *P* values less than 0.05 were considered statistically significant.

**Study approval.** This study was approved by the institutional review boards of Osaka University (approval number 681), University of Ulm (approval numbers 279/09 and 188/16), and University of Berlin (approval number EA2/077/12).

**Data sharing statement.** All data supporting the findings are available from the corresponding authors.

## Author contributions

BH, YM, NI, HS, PMK, and TK designed research. YM, MO, AK, TH, S Murata, TE, MJ, RF, and AH performed research. BH, MK, MA, S Murase, YU, and NK acquired the data. BH, YM, MO, MK, JN, YK, NK, HS, and PMK analyzed data. BH, YM, MO, HS, PMK, and TK wrote the paper. Three authors sharing the first author position are in alphabetical order.

## Acknowledgments

We thank Morihisa Fujita (Jiangnan University), Tatsutoshi Nakahata (Kyoto University), Hidenori Ohnishi (Gifu University), Tatsuya Saitoh (Tokushima University), and Yusuke Maeda (Osaka University) for discussion; Jean-Francois Dubremetz (Montpellier University) for T5-4E10 mAb; Lucio Luzzatto (Muhimbili University) for critical reading and editing advice on this manuscript; Keiko Kinoshita (Osaka University), Kana Miyanagi (Osaka University), Saori Umeshita (Osaka University), and Miguel Rodriguez de los Santos (University of Ulm) for technical help; Lisa A. Gerdes (Munich University) for collaboration regarding patient G3; and the patients for providing blood samples and pictures. We thank Edanz ([www.edanzediting.com](http://www.edanzediting.com)) for editing the English text of a draft of this manuscript. This work was supported by the Japan Society for Promotion of Sciences and The Ministry of Education, Culture, Sports, Science and Technology of Japan KAKENHI grants (JP16H04753 and JP17H06422) to TK, and a grant from the Japan Society of Complement Research to YM.

Address correspondence to: Taroh Kinoshita, Yabumoto Department of Intractable Disease Research, Research Institute for Microbial Diseases, Osaka University, 3-1 Yamada-oka, Suita, Osaka 565-0871, Japan. Phone: 81.6.6879.8328; Email: [tkinoshi@biken.osaka-u.ac.jp](mailto:tkinoshi@biken.osaka-u.ac.jp). Or to: Peter M. Krawitz, Institute for Genomic Statistics and Bioinformatics, Rheinische Friedrich-Wilhelms-Universität, Sigmund-Freud Street 25, 53127 Bonn, Germany. Phone: 49.228.287.14799; Email: [pkrawitz@uni-bonn.de](mailto:pkrawitz@uni-bonn.de). Or to: Hubert Schrezenmeier, Institute of Transfusion Medicine, University of Ulm and Institute of Clinical Transfusion Medicine and Immunogenetics, German Red Cross Blood Transfusion Service and University Hospital Ulm, Helmholtzstrasse 10, 89081 Ulm, Germany. Phone: 49.731.150.550; Email: [h.schrezenmeier@blutspende.de](mailto:h.schrezenmeier@blutspende.de).

- Parker C, et al. Diagnosis and management of paroxysmal nocturnal hemoglobinuria. *Blood*. 2005;106(12):3699-3709.
- Hill A, DeZern AE, Kinoshita T, Brodsky RA. Paroxysmal nocturnal haemoglobinuria. *Nat Rev Dis Primers*. 2017;3:17028.
- Takeda J, et al. Deficiency of the GPI anchor caused by a somatic mutation of the *PIG-A* gene in paroxysmal nocturnal hemoglobinuria. *Cell*. 1993;73(4):703-711.
- Hillmen P, et al. The complement inhibitor eculizumab in paroxysmal nocturnal hemoglobinuria. *N Engl J Med*. 2006;355(12):1233-1243.
- Hillmen P, et al. Long-term safety and efficacy of sustained eculizumab treatment in patients with paroxysmal nocturnal haemoglobinuria. *Br J Haematol*. 2013;162(1):62-73.
- Kinoshita T. Biosynthesis and deficiencies of glycosylphosphatidylinositol. *Proc Jpn Acad, Ser B, Phys Biol Sci*. 2014;90(4):130-143.
- Krawitz PM, et al. A case of paroxysmal nocturnal hemoglobinuria caused by a germline mutation and a somatic mutation in *PIGT*. *Blood*. 2013;122(7):1312-1315.
- Kawamoto M, Murakami Y, Kinoshita T, Kohara N. Recurrent aseptic meningitis with *PIGT* mutations: a novel pathogenesis of recurrent meningitis successfully treated by eculizumab. *BMJ Case Rep*. 2018;2018:bcr-2018-225910.
- Ohishi K, Inoue N, Kinoshita T. *PIG-S* and *PIG-T*, essential for GPI anchor attachment to proteins, form a complex with *GAA1* and *GPI8*. *EMBO J*. 2001;20(15):4088-4098.

10. Wang Y, Hirata T, Maeda Y, Murakami Y, Fujita M, Kinoshita T. Free, unlinked glycosylphosphatidylinositols on mammalian cell surfaces revisited. *J Biol Chem*. 2019;294(13):5038–5049.
11. Nakashima M, et al. Novel compound heterozygous PIGT mutations caused multiple congenital anomalies-hypotonia-seizures syndrome 3. *Neurogenetics*. 2014;15(3):193–200.
12. Bench AJ, et al. Chromosome 20 deletions in myeloid malignancies: reduction of the common deleted region, generation of a PAC/BAC contig and identification of candidate genes. UK Cancer Cytogenetics Group (UKCCG). *Oncogene*. 2000;19(34):3902–3913.
13. Aziz A, et al. Cooperativity of imprinted genes inactivated by acquired chromosome 20q deletions. *J Clin Invest*. 2013;123(5):2169–2182.
14. Araten DJ, et al. Cytogenetic and morphological abnormalities in paroxysmal nocturnal haemoglobinuria. *Br J Haematol*. 2001;115(2):360–368.
15. Sloand EM, et al. Cytogenetic abnormalities in paroxysmal nocturnal haemoglobinuria usually occur in haematopoietic cells that are glycosylphosphatidylinositol-anchored protein (GPI-AP) positive. *Br J Haematol*. 2003;123(1):173–176.
16. Li J, Bench AJ, Vassiliou GS, Fourouclas N, Ferguson-Smith AC, Green AR. Imprinting of the human L3MBTL gene, a polycomb family member located in a region of chromosome 20 deleted in human myeloid malignancies. *Proc Natl Acad Sci USA*. 2004;101(19):7341–7346.
17. Miyata T, et al. The cloning of PIG-A, a component in the early step of GPI-anchor biosynthesis. *Science*. 1993;259(5099):1318–1320.
18. Tomavo S, et al. Immunolocalization and characterization of the low molecular weight antigen (4–5 kDa) of *Toxoplasma gondii* that elicits an early IgM response upon primary infection. *Parasitology*. 1994;108(Pt 2):139–145.
19. Hirata T, et al. Identification of a Golgi GPI-N-acetylgalactosamine transferase with tandem transmembrane regions in the catalytic domain. *Nat Commun*. 2018;9(1):405.
20. Murakami Y, et al. Mechanism for release of alkaline phosphatase caused by glycosylphosphatidylinositol deficiency in patients with hyperphosphatasia mental retardation syndrome. *J Biol Chem*. 2012;287(9):6318–6325.
21. Buckley JT. The channel-forming toxin aerolysin. In: Alouf JE, Freer JH, eds. *The Comprehensive Sourcebook of Bacterial Protein Toxins*. London, England: Academic Press; 1999:362–372.
22. Kooyman DL, et al. In vivo transfer of GPI-linked complement restriction factors from erythrocytes to the endothelium. *Science*. 1995;269(5220):89–92.
23. Dunn DE, et al. A knock-out model of paroxysmal nocturnal hemoglobinuria: Pig-a(-) hematopoiesis is reconstituted following intercellular transfer of GPI-anchored proteins. *Proc Natl Acad Sci USA*. 1996;93(15):7938–7943.
24. Brodsky RA, et al. Improved detection and characterization of paroxysmal nocturnal hemoglobinuria using fluorescent aerolysin. *Am J Clin Pathol*. 2000;114(3):459–466.
25. Diep DB, Nelson KL, Raja SM, Pleshak EN, Buckley JT. Glycosylphosphatidylinositol anchors of membrane glycoproteins are binding determinants for the channel-forming toxin aerolysin. *J Biol Chem*. 1998;273(4):2355–2360.
26. Abrami L, et al. The glycan core of GPI-anchored proteins modulates aerolysin binding but is not sufficient: the polypeptide moiety is required for the toxin-receptor interaction. *FEBS Lett*. 2002;512(1-3):249–254.
27. Hong Y, et al. Requirement of N-glycan on GPI-anchored proteins for efficient binding of aerolysin but not *Clostridium septicum* alpha-toxin. *EMBO J*. 2002;21(19):5047–5056.
28. Parzych K, Zetterqvist AV, Wright WR, Kirkby NS, Mitchell JA, Paul-Clark MJ. Differential role of pannexin-1/ATP/P2X<sub>2</sub> axis in IL-1 $\beta$  release by human monocytes. *FASEB J*. 2017;31(6):2439–2445.
29. Ricklin D, Hajishengallis G, Yang K, Lambris JD. Complement: a key system for immune surveillance and homeostasis. *Nat Immunol*. 2010;11(9):785–797.
30. Sumichika H, et al. Identification of a potent and orally active non-peptide C5a receptor antagonist. *J Biol Chem*. 2002;277(51):49403–49407.
31. Fujita T, Endo Y, Nonaka M. Primitive complement system—recognition and activation. *Mol Immunol*. 2004;41(2-3):103–111.
32. Fujita T, Matsushita M, Endo Y. The lectin-complement pathway—its role in innate immunity and evolution. *Immunol Rev*. 2004;198:185–202.
33. Kvarnung M, et al. A novel intellectual disability syndrome caused by GPI anchor deficiency due to homozygous mutations in PIGT. *J Med Genet*. 2013;50(8):521–528.
34. Lam C, et al. Expanding the clinical and molecular characteristics of PIGT-CDG, a disorder of glycosylphosphatidylinositol anchors. *Mol Genet Metab*. 2015;115(2-3):128–140.
35. Skauli N, et al. Novel PIGT variant in two brothers: expansion of the multiple congenital anomalies-hypotonia seizures syndrome 3 phenotype. *Genes (Basel)*. 2016;7(12):E108.
36. Pagnamenta AT, et al. Analysis of exome data for 4293 trios suggests GPI-anchor biogenesis defects are a rare cause of developmental disorders. *Eur J Hum Genet*. 2017;25(6):669–679.
37. Kohashi K, et al. Epileptic apnea in a patient with inherited glycosylphosphatidylinositol anchor deficiency and PIGT mutations. *Brain Dev*. 2018;40(1):53–57.
38. Yang L, et al. Homozygous PIGT mutation lead to multiple congenital anomalies-hypotonia seizures syndrome 3. *Front Genet*. 2018;9:153.
39. Bayat A, et al. PIGT-CDG, a disorder of the glycosylphosphatidylinositol anchor: description of 13 novel patients and expansion of the clinical characteristics. *Genet Med*. 2019;21(10):2216–2223.
40. Lek M, et al. Analysis of protein-coding genetic variation in 60,706 humans. *Nature*. 2016;536(7616):285–291.
41. Rotoli B, Luzzatto L. Paroxysmal nocturnal hemoglobinuria. *Semin Hematol*. 1989;26(3):201–207.
42. Young NS. The problem of clonality in aplastic anemia: Dr Dameshek's riddle, restated. *Blood*. 1992;79(6):1385–1392.
43. Luzzatto L, Bessler M, Rotoli B. Somatic mutations in paroxysmal nocturnal hemoglobinuria: a blessing in disguise? *Cell*. 1997;88(1):1–4.
44. Inoue N, et al. Molecular basis of clonal expansion of hematopoiesis in 2 patients with paroxysmal nocturnal hemoglobinuria (PNH). *Blood*. 2006;108(13):4232–4236.
45. Shen W, et al. Deep sequencing reveals stepwise mutation acquisition in paroxysmal nocturnal hemoglobinuria. *J Clin Invest*. 2014;124(10):4529–4538.
46. Luzzatto L, Risitano AM. Advances in understanding the pathogenesis of acquired aplastic anaemia. *Br J Haematol*. 2018;182(6):758–776.
47. Neven B, Prieur AM, Quartier dit Maire P. Cryopyrinopathies: update on pathogenesis and treatment. *Nat Clin Pract Rheumatol*. 2008;4(9):481–489.
48. Saito M, et al. Disease-associated CIAS1 mutations induce monocyte death, revealing low-level mosaicism in mutation-negative cryopyrin-associated periodic syndrome patients. *Blood*. 2008;111(4):2132–2141.
49. Faustmann PM, Krause D, Dux R, Dermietzel R. Morphological study in the early stages of complement C5a fragment-induced experimental meningitis: activation of macrophages and astrocytes. *Acta Neuropathol*. 1995;89(3):239–247.
50. Herz J, Filiano AJ, Smith A, Yoge N, Kipnis J. Myeloid cells in the central nervous system. *Immunity*. 2017;46(6):943–956.
51. An LL, et al. Complement C5a potentiates uric acid crystal-induced IL-1 $\beta$  production. *Eur J Immunol*. 2014;44(12):3669–3679.
52. Samstad EO, et al. Cholesterol crystals induce complement-dependent inflammasome activation and cytokine release. *J Immunol*. 2014;192(6):2837–2845.
53. Laudisi F, et al. Cutting edge: the NLRP3 inflammasome links complement-mediated inflammation and IL-1 $\beta$  release. *J Immunol*. 2013;191(3):1006–1010.
54. Arbore G, et al. T helper 1 immunity requires complement-driven NLRP3 inflammasome activity in CD4<sup>+</sup> T cells. *Science*. 2016;352(6292):aad1210.
55. Hong Y, et al. Human PIG-U and yeast Cdc91p are the fifth subunit of GPI transamidase that attaches GPI-anchors to proteins. *Mol Biol Cell*. 2003;14(5):1780–1789.
56. Sugita Y, et al. Recombinant soluble CD59 inhibits reactive haemolysis with complement. *Immunology*. 1994;82(1):34–41.
57. Nakamura N, et al. Expression cloning of PIG-L, a candidate N-acetylglucosaminylphosphatidylinositol deacetylase. *J Biol Chem*. 1997;272(25):15834–15840.
58. Morath S, Geyer A, Hartung T. Structure-function relationship of cytokine induction by lipoteichoic acid from *Staphylococcus aureus*. *J Exp Med*. 2001;193(3):393–397.
59. Martinon F, Pétrilli V, Mayor A, Tardivel A, Tschopp J. Gout-associated uric acid crystals activate the NALP3 inflammasome. *Nature*. 2006;440(7081):237–241.
60. Zhou R, Yazdi AS, Menu P, Tschopp J. A role for mitochondria in NLRP3 inflammasome activation. *Nature*. 2011;469(7329):221–225.
61. Matsushita M, et al. A novel human serum lectin with collagen- and fibrinogen-like domains that functions as an opsonin. *J Biol Chem*. 1996;271(5):2448–2454.